Adv. Polar Upper Atmos. Res., **14**, 128–137, 2000

Meridional gradients of the neutral temperature in the dayside summer *E*-region

Sawako Maeda[1*] and Satonori Nozawa[2]

[1]*Kyoto University of Art and Design, 2-116 Uryuyama, Kitashirakawa, Sakyo-ku, Kyoto 606-8271*
[2]*Solar-Terrestrial Environment Laboratory, Nagoya University, Chikusa-ku, Nagoya 464-8601*

Abstract: A special measurement using the European Incoherent Scatter (EISCAT) UHF radar was conducted on July 01, 1998 to observe the dayside summer *E*-region meridional temperature gradient. The purpose of this study is to examine whether the temperature gradient obtained from the direct temperature measurement is consistent with the temperature gradient deduced from the neutral velocity measured by the EISCAT Common Program 2 (CP-2) (S. Maeda *et al.*, J. Geophys. Res., **104**, 19871, 1999). It is suggested that the meridional temperature gradient lay in the range between − 0.2 K/km and 0.2 K/km from 99 to 108 km heights in spite of rather large errors of about 0.1 K/km arising from various causes. The magnitude was about 4 times greater than that deduced from the CP-2 data. A lack of consistency between them was attributed to the fact that the former one represented rather instantaneous data, but the latter was hourly averaged. The measured neutral velocity is also presented.

1. Introduction

The momentum balance in the *E*-region is characterized primarily by the so-called geostrophic balance between the Coriolis force and the pressure gradient force. The drags due to the viscosity owing to the molecular and eddy diffusion and the ion-neutral collisions as well as the tidal forcing also affect the momentum balance. The so-called "wave-drag" that is related to the momentum flux convergence due to a breaking gravity wave plays an important role on the neutral dynamics in the lower *E*-region (Vial and Forbes, 1989; Miyahara and Forbes, 1991).

Optical rocket experiments for high-latitude neutral wind measurements revealed vertical shears which exceeded 150 m/s over a height range of 2.5 km (Larsen *et al.*, 1995). These features are not predicted by any tidal models nor by the simulation of the high latitude forcing (Brinkman *et al.*, 1995). Although the optical experiments are restricted to nighttime measurements, an incoherent scatter radar gives us daytime measurements of the lower thermospheric winds. The European Incoherent Scatter (EISCAT) UHF radar (Folkestad *et al.*, 1983) is also capable of being used for the nighttime measurements. It is feasible to study the momentum balance relating to the dayside vertical velocity shears by using the EISCAT radar data.

The EISCAT UHF radar system provides observations of various key parameters of the ionosphere and the thermosphere (Fujii *et al.*, 1998; Virdi and Williams, 1993). The

* Present address: Kyoto Women's University, 35 Kitahiyoshi, Imakumano, Higashiyama-ku, Kyoto 606-8501.

Table 1. Characteristics of the EISCAT UHF Radar at Tromsø.

Geographical coordinates	69°35'N, 19°14'E
Invariant latitude	66°12'N
Frequency (MHz)	931
Maximum bandwidth (MHz)	8
Peak power (MW)	1.5
Pulse duration (ms)	.001–1.0
Minimum interpulse (ms)	1.0
Gain (dBi)	48
System temperature (K)	90–110

(Annual Report 1996–1997, EISCAT Scientific Association)

technical characteristics and operational capabilities were outlined in Folkestad *et al.* (1983). In Table 1 the characteristics of the radar system are quoted (after Annual Report 1996–1997, EISCAT Scientific Association, 1999). EISCAT's common programmes can be used in the three way to assess the neutral dynamics: the tristatic method (Common Programme 1:CP-1), the beamswinging method (Common Programme 2: CP-2) and the field-aligned method (both CP-1 and CP-2) (A recent description about the EISCAT's common programmes can be found in Collis, 1995). Williams *et al.* (1994) compared the capabilities of the three methods, and concluded that the CP-2 mode (the beamswinging method) can determine reliably the vector of neutral winds in the lower thermosphere with a height resolution of 4.5 km which is two times higher than that of the CP-1 mode (the tristatic method).

The *E*-region neutral winds were analyzed previously by using data from EISCAT CP-2 at the quiet summer daytime (Maeda *et al.*, 1999, hereafter referred to as Paper 1). The neutral horizontal velocity was derived from the steady-state ion momentum equation neglecting the ambipolar diffusion (Rino *et al.*, 1977):

$$\mathbf{U} = \mathbf{v}_i - \Omega_i (\mathbf{E} + \mathbf{v}_i \times \mathbf{B}) / (|\mathbf{B}| \nu_{in}), \quad (1)$$

where $\Omega_i = e|\mathbf{B}|m_i^{-1}$, $\mathbf{U}$ is the neutral horizontal velocity, $\mathbf{v}_i$ is the ion velocity, $\mathbf{B}$ is the magnetic field, $\mathbf{E}$ is the electric field, m_i is the ion mass, e is the electric charge, and ν_{in} is the ion-neutral collision frequency. By using the neutral momentum equation, the pressure gradient force was estimated from the neutral velocity. The results are reviewed in Section 2. In the present paper, it is examined whether the temperature gradient deduced in Paper 1 will actually be observed in similar conditions of season, local time and geomagnetic activity. The program of the measurement is described in Section 3. The results of the measurement are presented in Section 4. The conclusions are given in Section 5.

2. *E*-region neutral momentum balance

Paper 1 examined the degree to which the *E*-region neutral wind was quasi-

geostrophic directly from the measurements of the neutral velocity, electric field and electrical conductivities via the time-dependent neutral momentum equation,

$$-\nabla P/\rho = 2\Omega \times \mathbf{U} + d\mathbf{U}/dt - (\mathbf{J} \times \mathbf{B})/\rho - \mu(\partial^2 \mathbf{U}/\partial z^2)/\rho, \quad (2)$$

where, P is the pressure, ρ is the atmospheric density, Ω is the angular velocity of the Earth rotation, $\mathbf{J}$ is the current density, and μ is the viscosity coefficient including the molecular and eddy viscosity. The "wave drag" due to the gravity wave breaking, however, was not taken into account because it is important mainly around 80 km height, and highly variable at high latitude (Holton, 1982; Fritts, 1995). Furthermore, the uncertainty concerning the gravity wave breaking should be avoided. Another reason for this was about 70% of the total flux due to the gravity wave forcing was accounted for in wave periods of less than one hour (Fritts, 1995). The neutral velocity and the corresponding pressure gradient force were obtained in the hourly average basis.

The quiet-time dayside momentum balance was summarized as follows:

(1) The Coriolis force was greater than the other forcings below 116 km height, and the ion drag was much smaller than the others.
(2) The viscous force should be important above 116 km height because of the large velocity shear and the low air density.
(3) The acceleration $d\mathbf{U}/dt$ was the same order of magnitude as that of the pressure gradient force and the Coriolis force below 106 km height.
(4) The absolute magnitude of the pressure gradient force that was estimated by the eq. (2) was less than 0.02 m/s^2.

In conclusion, it was suggested that the Coriolis force and the pressure gradient force were the dominant forces between 110 and 116 km height. Furthermore, it is found that the pressure gradient force of 0.02 m/s^2 corresponds to a temperature gradient of about 0.05 K/km via the relation, $\nabla T = (m_0/R_0 \rho)\nabla P$, where T is the temperature, R_0 is the gas constant, and m_0 is the mean molecular mass.

3. Measurements

Meridional gradients of the neutral temperature and the neutral winds in the dayside summer *E*-region were measured by the EISCAT UHF radar between 0801 UT (0901 LT and 1001 MLT) and 1257 UT (1357 LT and 1457 MLT) on July 01, 1998. An antenna cycle is shown in Table 2. The antenna position was changed from FA, S, SE, South, FA, S, SE, and North in a cycle. The directions of FA, S, SE were the same as those of the Tromsø antenna positions in the CP-2 experiment (Williams *et al.*, 1994). The azimuth and elevation for each beam are listed in Table 2. The cycle time was 50 min. The electric field was obtained by the tristatic method at 278 km height at the FA, South and North positions. The ion temperature analyzed in the present paper was also measured at these three positions. The dwell times at the FA, South and North positions were about 380, 770, and 795 s, respectively. Together with the S and SE data, the FA data in the last 60 s were also used for the monostatic measurements of the ion velocity. The observed error involved in fitting a theoretical autocorrelation function to the observed one is also shown in Table 2, which ranged from 5 to 25 K between 98 and

Table 2. Antenna positions in the 50 min repeat cycle.

Position	Azimuth (°)	Elevation (°)	Dwell time (s)	Moving time (s)	Parameter	Ti-error (K)	Mode
FA	183.2	77.2	320		Ti, E	5–16	Tristatic
			60	20			Monostatic
S	166.5	62.9	60	30	Vi		Monostatic
SE	133.3	60.4	60	40			Monostatic
South	180.0	30.0	770	40	Ti, E	7–25	Tristatic
FA	183.2	77.2	320		Ti, E	5–16	Tristatic
			60	20			Monostatic
S	166.5	62.9	60	30	Vi		Monostatic
SE	133.3	60.4	60	110			Monostatic
North	0.0	30.0	795	145	Ti, E	7–23	Tristatic

115 km height. The horizontal distance between the antenna positions of North and South beams was about 330 km at 99 km height and about 400 km at 120 km height (Fig. 1).

The meridional gradient of the neutral temperature was derived under the assumption of equality of the ion and neutral temperatures below 115 km height. The assumption is verified when neutral gas attains thermal equilibrium with the ions under the condition of small electric field of less than a few tens of mV/m (Banks and Kockarts, 1973; Schunk and Sojka, 1982; Kofman, 1992). The ion temperature may be higher than the neutral one due to the energetic photoelectrons during dayside summer time (Rees, 1989). In the present paper, however, the conclusions would not be much affected by the assumption because the paper is concerned not with the absolute

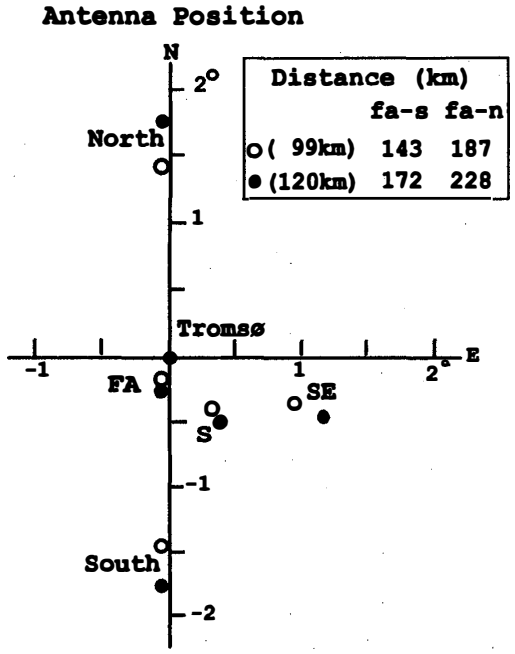

Fig. 1. Antenna positions of five beams (North, South, FA, S, SE) at Tromsø employed for the measurements in July 01, 1998. An open circle shows the position at 99 km height, a closed one at 120 km height, respectively. The elevation angle and azimuth of each beam are referred to Table 2. The horizontal distances between the positions of FA and South beams and between the positions of FA and North beams are also shown.

magnitude of the temperature but with the difference between the temperatures at the various positions. The effects of the photoelectrons would be rather uniform over the region.

4. Results and discussions

The measurement was conducted during a geomagnetic quiet period. The 3-hourly K_p index was between 0^+ and 1. The electric fields measured tristatically at the FA, North and South positions were less than 5 mV/m throughout the period. Figure 2 shows the results of the temperature measurements with the North and South beams at each height level from 99 to 115 km. A closed circle shows the temperature at the South position with the observed error and an open one at the North position, respectively. The temperature at the FA position is also shown by a small triangle. Note that the ranges of the vertical axes at each height are not the same.

The temperature at the FA position was fitted by a polynomial function to interpolate to at any given time. Then the difference between the interpolated temperature at the FA position and the temperature at the North position, and the difference between the temperature at the South position and the interpolated temperature at the FA position were calculated at each time. There were some data gaps due to system failure. Since the observed error was significantly large between 0945 UT and 1032 UT, the FA data at these times were excluded from the polynomial fitting. A best-fit polynomial was determined from a χ^2-test for the significance level of 90%. At 108 km height, the polynomial of the order of 3 was chosen before 1130 UT, and order 5 after that time. The best-fit polynomials are also shown by the dotted lines. Table 3 presents the order of the best-fit polynomials and the standard deviation. The error total shown in Table 3 is the square root of the sum of the square of the observed error shown in Table 2 and the square of the standard deviation in the polynomial fitting (Williams *et al.*, 1996). Considering the observed error in the temperatures at the North and South positions, it is noted that the temperature difference between the North (South) position and the FA position should not be statistically significant if it is less than 16 K at 99 km height and 40 K at 115 km height. The temperature difference between the three positions lay in the range between –11 K and 32 K at 99 km height and between –56 K and 40 K at 115 km height, respectively. The temperature difference fluctuated with time. It is not easy to find the significance of the temperature difference due to the rather large errors at each height.

The meridional temperature gradient is shown in Fig. 3. The unit is K/km. Positive value means southward, that is, the southern temperature is higher than the northern temperature. Although the direction of the temperature gradient varied rather randomly, the range of the magnitude was similar at the six height levels. The absolute magnitude was mostly less than 0.2 K/km. The range from –0.2 to 0.2 K/km was 4 times greater than that deduced from the neutral velocity in Paper 1. The overall error level in the temperature gradient was in the order of about 0.1 K/km at 99 km height, and of 0.2 K/km at 115 km height. In this sense, many of the data were below the error level, particularly above 112 km height. It is still meaningful that the range was from –0.2 to 0.2 K/km in the lower region, because the errors in the lower region arose mainly from the polynomial fitting due to the rapid fluctuations of the temperature at the FA position.

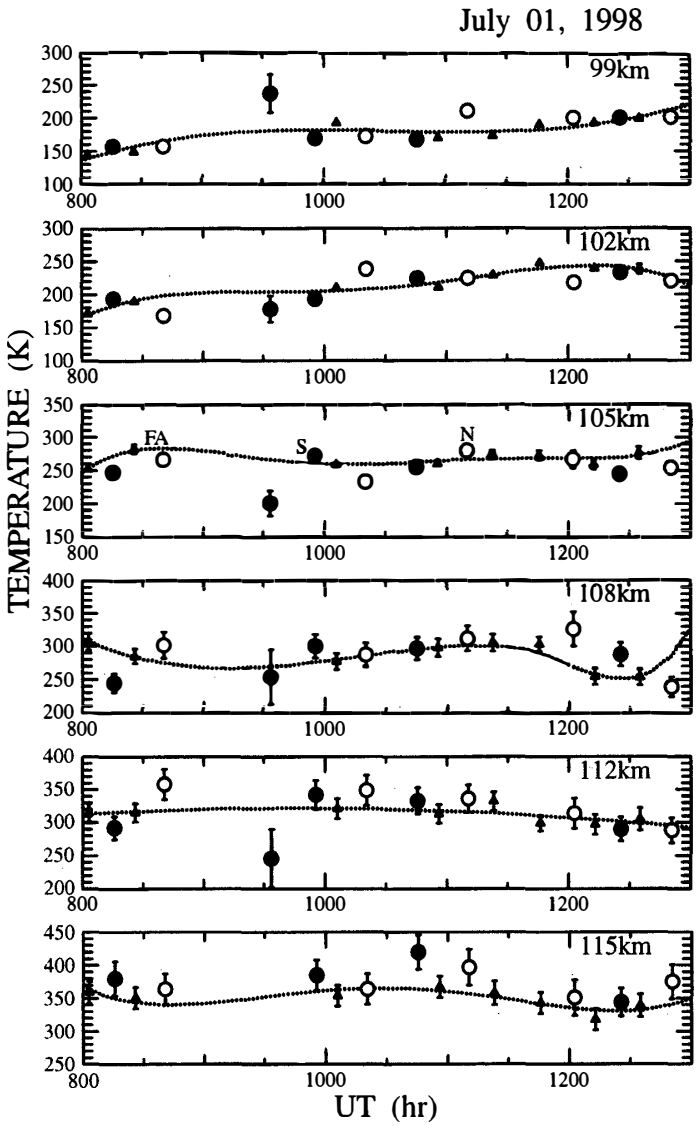

Fig. 2. Time variations of the neutral temperature at 6 levels from 99 to 115 km height. An open circle shows the temperature at the North position, and a closed circle at the South position, respectively. The temperature at FA position is also shown by a small triangle. The dotted lines are the best-fit polynomials to the temperature at FA position.

Table 3. Best-fit polynomial functions for the temperature at the FA position.

Height (km)	Order	Standard deviation for the significance level of 90% (K)	Error total (K)
99	3	7.0–18.0	9–19
102	4	5.3–13.4	7–14
105	5	6.7–17.2	8–18
108	3	8.1–20.6	14–24
	(5)	(11.5–29.4)	(14–32)
112	2	7.5–19.1	17–24
115	4	8.8–22.3	18–27

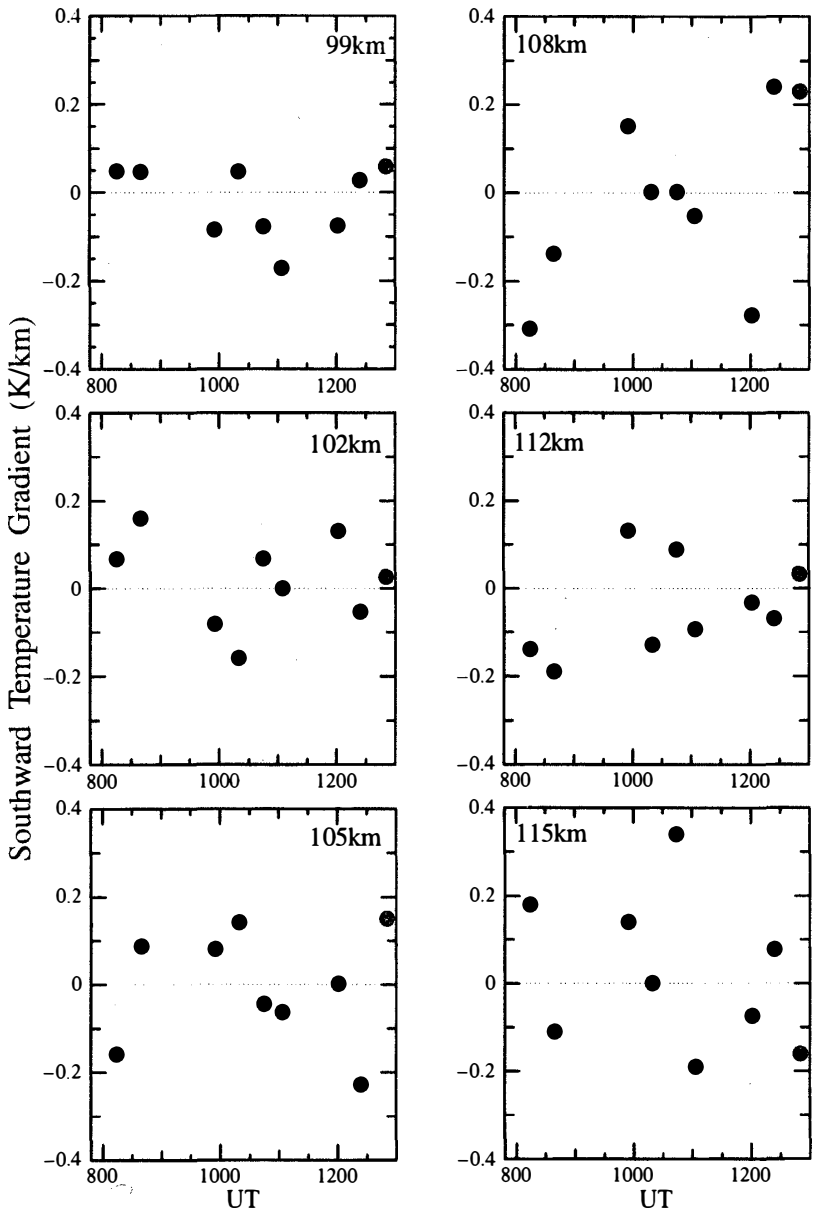

Fig. 3. Meridional temperature gradient at 6 levels from 99 to 115 km height. The unit is K/km. Positive value means the southward gradient, that is, the southern temperature is higher than the northern temperature.

It is suggested that the observed temperature difference may be associated with fluctuations with the time scale less than a few tens of minutes and/or with the spacial scale less than a few hundreds of km. In the lower *E*-region, the turbulence generated by the breaking gravity waves (Vial and Forbes, 1989) may induce rapid fluctuations and causes the random errors in the temperature fields.

The measured neutral velocity is shown in Fig. 4. The open and closed circles show the meridional and zonal components of the neutral velocity, respectively. Positive values are northward and eastward winds, respectively. Both of the meridional and the zonal winds lay in the range between –200 and 200 m/s. It seems that except for the highest

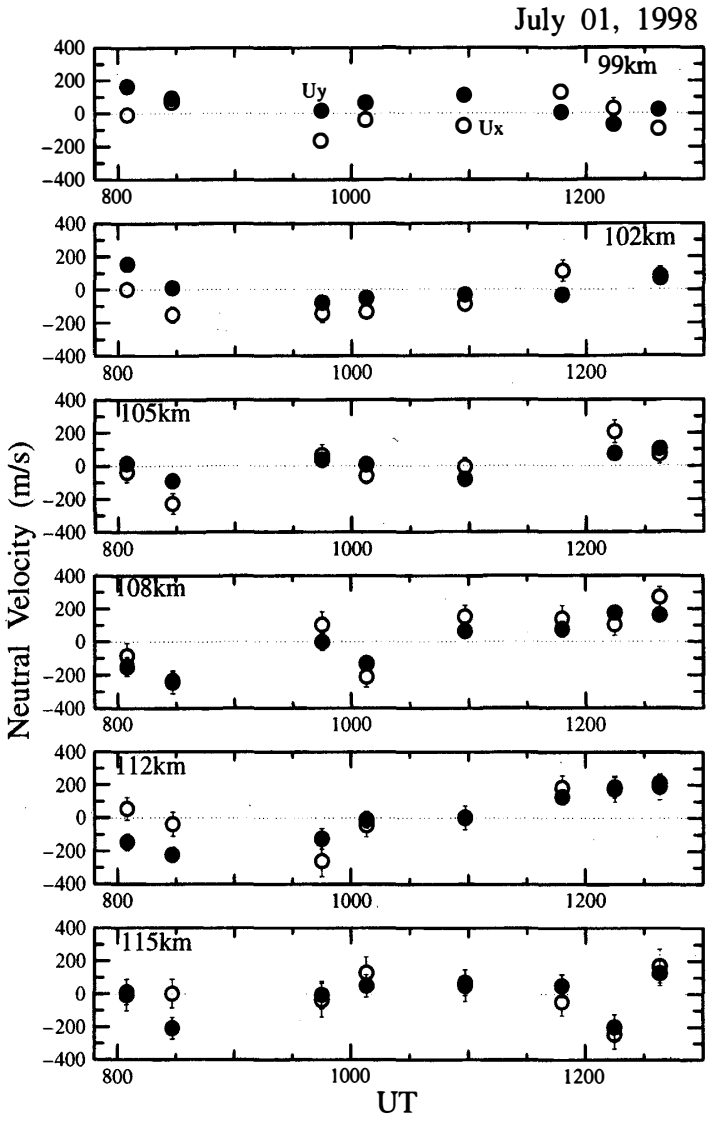

Fig. 4. Neutral velocity at 6 levels from 99 to 115 km height. An open circle shows the meridional component (U_x), and a closed circle the zonal components (U_y), respectively.

level of 115 km, the meridional wind was southward before about 1000 UT, and then turned northward. At the heights of 108 and 112 km, the zonal wind was westward before 1000 UT and then turned eastward. It seems likely that the vertical shears of the meridional and zonal winds were large. At present, whether the time variations of the neutral velocity related to the temperature variations is not revealed yet.

It is an interesting thing to compare the measured neutral velocity with the geostrophic winds $\mathbf{U}_g(=-\nabla P/2\rho\Omega\sin\theta$, θ is the latitude). The pressure gradient force was calculated from the temperature gradient via $-\nabla p=-(R_0\rho/m_0)\nabla T$. In principle, the geostrophic winds could be estimated from the temperature gradient observed here. However, it might not be valid since the geostophic balance is the concept under the condition of the quasi-steady state and the results discussed above did not support the quasi-steady state approximation for the present data set.

5. Conclusions

The EISCAT UHF measurements of the meridional distribution of the temperature were discussed. It was inferred that the temperature gradient below 112 km height lay in the range from –0.2 to 0.2 K/km, the overall errors arising from various causes were not small though. It was suggested that the temperature gradients represented the structures with the time scale less than a few tens minutes and/or with the spatial scale less than a few hundreds km.

A similar program of continuous measurements for more than 12 hours is highly desirable from the two points of view: the observed errors will be reduced largely by a smoothing procedure such as running averages, and the analyses of the tides and gravity waves would become possible by using the long duration data. The simultaneous observations using Tromsø UHF radar and the ESR would be suitable for these objectives as well.

Acknowledgments

We indebted to the Director and staff of EISCAT for operating the facility and supplying the data. EISCAT is jointly funded by the Particle Physics and Astronomy Research Council (U.K.), Centre National de la Recherche Scientifique (France), Max-Plank Gesellschaft (F.R.G.), Suomen Akatemia (Finland), National Institute of Polar Research (Japan), Norges Almenvitenskapelige Forskningsrad (Norway), and Naturvetenskapliga Forskningsradet (Sweden). The authors thank anonymous referees for their kind comments in reviewing the paper.

The editor thanks Drs. Shigeto Watanabe and Chris Hall for their help in evaluating this paper.

References

Banks, P.M. and Kockarts, G. (1973): Aeronomy. New York, Academic.

Brinkman, D.G., Walterscheid, R.L., Lyons, L.R., Kayser, D.C., Christensen, A.B., Sharber, J.R., Frahm, R.A. and Larsen, M.F. (1995): *E*-region neutral winds in the postmidnight diffuse aurora during the Atmospheric Response in Aurora I rocket campaign. J. Geophys. Res., **100**, 17309–17320.

Collis, P.N. (1995): EISCAT data base for ionospheric modelling: *F*-region and topside ionosphere. Adv. Space Res., **16** (1), 37–46.

Folkestad, K., Hagfors, T. and Westerlund, S. (1983): EISCAT: an updated description of technical characteristics and operational capabilities. Radio Sci., **18**, 867–879.

Fujii, R., Nozawa, S., Matuura, N. and Brekke, A. (1998): Study on neutral wind contribution to the electrodynamics in the polar ionosphere using EISCAT CP-1 data. J. Geophys. Res., **103**, 14731–14739.

Fritts, D.C. (1995): Gravity wave forcing and effects in the mesosphere and lower thermosphere. The Upper Mesosphere and Lower Thermosphere, ed. by R.M. Johnson and T.L. Killeen. Washington, D.C., Am. Geophys. Union, 89–100 (Geophys. Monogr. Ser., **87**).

Holton, J.R. (1982): The role of gravity wave induced drag and diffusion in the momentum budget of the mesosphere. J. Atmos. Sci., **39**, 791–799.

Kofman, W. (1992): Auroral ionospheric and thermospheric measurements using the incoherent scatter technique. Surv. Geophys., **13**, 551–571.

Larsen, M.F., Marshall, T.R., Mikkelsen, I.S., Emery, B.A., Christensen, A., Kayser, D., Hechet, J., Lyons, L. and Walterscheid, R. (1995): Atmospheric response in aurora experiment: Observations of *E* and *F* region neutral winds in a region of postmidnight diffuse aurora. J. Geophys. Res., **100**, 17299–17308.

Maeda, S., Fujiwara, H. and Nozawa, S. (1999): Momentum balance of dayside *E* region neutral winds during geomagnetically quiet summer days. J. Geophys. Res., **104**, 19871–19879.

Miyahara, S. and Forbes, J.M. (1991): Interactions between gravity waves and the diurnal propagation tide in the mesosphere and lower thermosphere. J. Meteorol. Soc. Jpn., **69**, 523–531.

Rees, M.H. (1989): Physics and Chemistry of the Upper Atmosphere. New York, Cambridge Univ. Press.

Rino, C.L., Brekke, A. and Baron, M.J. (1977): High-resolution auroral zone *E*-region neutral wind and current measurements by incoherent scatter radar. J. Geophys. Res., **82**, 2295–2304.

Schunk, R.W. and Sojka, J.J. (1982): Ion temperature in the daytime high-latitude *F* region. J. Geophys. Res., **87**, 5169–5183.

Vial, F. and Forbes, J.M. (1989): Recent progress in tidal modelling. J. Atmos. Terr. Phys., **51**, 663–671.

Virdi, T.S. and Williams, P.J.S. (1993): Altitude variations in the amplitude and phase of tidal oscillations at high latitude. J. Atmos. Terr. Phys., **55**, 697–717.

Williams, P.J.S., Virdi, T.S., Jones G.O.L. and Huuskonen, A. (1994): A comparison of three methods of measuring tidal oscillations in the lower thermosphere using EISCAT common programmes. J. Atmos. Terr. Phys., **56**, 1347–1359.

Williams, P.J.S., Etemadi, A., McCrea, I.W. and Todd, H. (1996): Errors due to random noise in velocity measurement using incoherent-scatter radar. Ann. Geophys., **14**, 1480–1486.

(Received October 25, 1999; Revised manuscript accepted February 25, 2000)